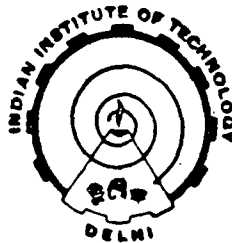


SOME STUDIES OF SEEDING AND CURRENT CONDUCTION IN MHD COMBUSTION PLASMAS

by

SUNIL CHANDRA SHARMA

Thesis submitted
to the
Indian Institute of Technology, Delhi
for the award of the degree of
DOCTOR OF PHILOSOPHY



Centre for Energy Studies
INDIAN INSTITUTE OF TECHNOLOGY, DELHI

Hauz Khas, New Delhi-110016

INDIA

December, 1986

TO MY PARENTS

CERTIFICATE

1) I am satisfied that the thesis presented by Mr. S. C. Sharma is worthy of consideration for the award of the degree of Doctor of Philosophy and is a record of the original bonafide research work carried out by him under my guidance and supervision and that the results contained in it have not been submitted in part or full to any other university or Institute for award of any degree/diploma.

2) I certify:

that he/she has pursued the prescribed course of research.

(Signature)
Chairman, D.R.C.

Sharma
20/11/88

Department of
I.I.T., Delhi.

Centre of Energy Studies

Meeliny
(Signature) 24/12/88
Supervisor of the Candidate

Address Dr R.P. Dahiya
Asstt Professor
Centre of Energy Stud

P.T.O.

ACKNOWLEDGEMENT

It gives me a great pleasure to express my profound sense of gratitude to Dr. R.P. Dahiya under whose supervision and guidance, I had the privilege to carry out my research work. I am indebted to him for his invaluable suggestions and constant encouragement.

I express my deep sense of gratitude to professor M.S. Sodha, Co-ordinator MHD group, for his generosity, inspiration and interest shown in my work. I sincerely thank Professor P.D. Grover, Head Centre of Energy studies and Professor K.L. Chopra, Department of physics for providing the experimental facilities. My thanks are due to Dr. A. Chandra Dr. B.K. Sawhney and Dr. Bhumesh Gupta for their helping attitude and encouragement.

I also thank Dr. Ami Chand, Dr. G.V.R. Raju, Dr. Ashok Sharma and Dr. Ashwani Kumar and Mr. Ashwani Metha for their friendly co-operation and helpful discussions. The Member of the workshop deserve special praise for their technical help. I am thankful to Mr. Kripal Singh for making neat drawings. I owe a deep sense of gratitude to my friend Mr. S.K. Jain and Colleagues of MHD and Plasma group.

Finally, I record gratitude to my father Mr. Jag Ram Singh Sharma, Mother Mrs. Murti Sharma and wife Archana for their abundant affection and co-operation provided to complete the job.

S.C. Sharma

(Sunil Chandra Sharma)

PREFACE

Magnetohydrodynamic (MHD) power generator in combination with a steam botting^{om} plant has the potential to give an overall efficiency upto 50 per cent. In an open cycle MHD power generator, fossil fuel is burnt with oxygen enriched air and the desired level of electrical conductivity of the combustion products is attained by adding a low ionization potential material, which is known as seed. Potassium carbonate is considered suitable for seeding the working fluid of open cycle MHD power generators.

In the present thesis, combustion and current conduction processes in seeded combustion plasma have been investigated under different physical conditions which may be relevant to gaseous fuel fired open cycle MHD power generators. Aqueous solution of potassium carbonate has been injected with the help of a two fluid pneumatic atomiser in the combustion products of liquefied-petroleum-gas (LPG, $C_{3.7}H_{8.8}$) and oxygen. The transport properties of potassium carbonate seeded combustion plasma, viz. composition, combustion temperature and electrical conductivity have been studied by incorporating the moles of water and potassium carbonate present in the aqueous seed solution. Investigations have also been made for the seed drop size distribution obtained from a pneumatic atomiser. It has been observed that the mean drop size gets lowered and distribution becomes more uniform on increasing the relative velocity between the aqueous seed solution and atomising oxygen at the interaction zone. The level of seed ionization has been observed to be influenced by the mean drop size.

The boundary layers developed over the copper and stainless steel (304) electrodes have been investigated for different sets of physical parameters, viz., electrode temperature, electrode surface conditions, applied voltage and seeding ratio (weight per cent of potassium). The alkali seed material present in the seeded plasma has been found to get adsorbed on the relatively cool electrode surfaces. A composite layer of low work function (~ 2.13 eV) has been observed

to be formed over the copper cathode facilitating thermionic emission of electrons. In diffusive mode of conduction, the anode potential drop, the cathode potential drop and the current density have been investigated as function of electrode (cathode/anode) temperature. For planar copper electrodes current density typically of 2400 amp/m^2 , for an applied voltage of 100 V has been achieved when the temperature of both the electrodes is around 1220 K. The current density has been observed to increase further up to 2800 amp/m^2 when matrix cathode with sharp multiple points is used under similar operating conditions. Experiments have also been conducted by using stainless steel (304) electrodes which are capable of sustaining temperatures higher than those of copper electrodes. The thermionic emission of electrons from the seed laden stainless steel cathode has been observed to give current density of the order ^{of} 3500 amp/m^2 , for electrode temperature of 1500 K and an applied voltage of 60 volts. Under these conditions, a potential drop of 25 volt has been observed to appear in anode electrostatic sheath, after seven hours of channel run time.

Temporal behaviour of the metallic electrodes has been investigated as a function of channel run time. When we start with the fresh copper electrodes, their surfaces get coverage of seed compound over a period of time. Adsorption of potassium is uniform on both the electrodes but the cathode surface get enhanced seed coverage due to additional contribution made by positively charged potassium ions drifting towards it from the plasma core. The anode potential drop then increases appreciably. It has been observed that after 16 hours of channel run time, 70 per cent of applied voltage drop in anode boundary region.

The composite surfaces formed on the electrodes are investigated by Auger Electron Spectroscopic, Differential Thermal Analysis and Scanning Electron Microscopic techniques. The material adsorbed on the electrode surfaces has been found to be primarily potassium carbonate.

LIST OF FIGURE

		Page
Fig 1.1	Schematic diagram showing the principle of MHD power generation.	2
Fig 2.1	Schematic diagram showing different stages involved in the evaporation of an aqueous seed droplet.	19
Fig 3.1	Photograph of experimental system.	36
Fig 3.2	Schematic diagram of experimental set up.	37
Fig 3.3	Burner with pneumatic atomiser fixed concentrically.	39
Fig 3.4	Seed injection system.	41
Fig 3.5	Two fluid pneumatic atomiser.	42
Fig 3.6	Schematic diagram showing electrodes placed in the test section.	48
3.7(a)	Rectangular cross section copper electrodes.	50
3.7(b)	Cylindrical cross section stainless steel electrodes.	50
Fig 3.8	Matrix Copper cathode with an array of 65 points.	51
Fig 3.9	Four probe assembly fixed inside the test section.	56
Fig 3.10	Circuit diagram for simultaneous recording of current, cathode drop (V_C) and anode drop (V_a).	58
Fig 4.1	Variation of measured relative number density as a function of drop diameter. The dashed curve shows the Nukiyama - Tanasawa plot for a mean diameter of 40 microns.	62

	Page
Fig 4.2	Variation of fractional radius of a seed drop with t/r_0^2 during the seven stages involved in evaporation. 64
Fig 4.3	Variation of potassium evaporation percentage with square root of time ($t^{1/2}$) for different mean radii marked on the respective curves. 66
Fig 4.4	Variation of potassium evaporation percentage with square root of time for different flame temperatures. 67
	(a) Atomising oxygen flow rate, $Q_A=3.3$ litre/min 67
	(b) Atomising oxygen flow rate, $Q_A=3.8$ litre/min 68
	(c) Atomising oxygen flow rate, $Q_A=4.3$ litre/min 69
Fig 4.5	Variation of potassium evaporation percentage with axial distance from the burner at constant weight per cent of potassium for different flame temperatures. 71
Fig 4.6	Variation of experimentally measured temperature along the channel for different values of atomising oxygen flow rate (Q_A). 72
Fig 4.7	Analytically evaluated combustion temperature and electrical conductivity corresponding to different flow rates of aqueous seed solution keeping $\epsilon = 1.0$. 74
Fig 4.8	Variation of theoretical electrical conductivity as a function of seeded combustion plasma temperature. 75
Fig 4.9	Variation of analytically evaluated electrical conductivity as a function of seeded combustion plasma temperature for different values of weight per cent of potassium, 15 per cent aqueous seed solution is used to achieve the desired value of ϵ . 76

	Page
Fig 4.10	78
Variation of experimentally measured electrical conductivity along the channel for different flow rates of atomising oxygen. The analytically evaluated electrical conductivity is represented by the dashed curve.	
Fig 4.11	79
Variation of temperature and electrical conductivity as a function of atomising oxygen flow rate measured at different points along the channel marked on the respective curves. The analytically evaluated conductivity is represented by the dashed curve.	
Fig 4.12	81
Electrical conductivity measured with four probe method. The dashed curve represents the analytically evaluated conductivity at a distance of 16 cm from the burner.	
Fig 5.1	85
Variation of current density as a function of anode temperature $T_C = 960$ K and $\epsilon = 0.0$.	
Fig 5.2	87
Variation of current density as a function of cathode temperature. $T_a = 900$ K and $\epsilon = 0.0$	
Fig 5.3	89
Variation of anode potential drop as a function of anode temperature, $T_C = 940$ K $\epsilon = 0.632$.	
Fig 5.4	90
Variation of cathode potential drop as a function of anode temperature, $\epsilon = 0.632$ and $T_C = 940$ K .	
Fig 5.5	91
Variation of plasma potential drop (V_p) and current density (J) as a function of anode temperature, $\epsilon = 0.451$, $T_C = 1250$ K, $V_{app} = 40$ V and Plasma temperature = 2700K	
Fig 5.6	93
Variation of anode potential drop with channel run time. $\epsilon = 0.495$, $T_C = T_a = 1250$ K, $V_{app} = 80$ V.	
Fig 5.7	95
Variation of the anode potential drop with channel run time. The curves are marked with respective applied voltages, $\epsilon = 0.495$ $T_C = T_a = 1250$ K.	

	Page
Fig 5.8 Potential distribution between the electrodes. $\epsilon = 0.442$ and $V_{app} = 80V$. Position of probes is marked by numbers 1 to 6.	96
Fig 5.9 Current - Voltage characteristics in diffusive mode of conduction for different electrode temperatures.	98
Fig 5.10 Variation of anode potential drop and cathode potential drop as a function of current density for different electrode temperatures.	99
Fig 5.11 (a) Variation of current density as a function of cathode temperature measured after 3 hours of channel run time. The dashed line represents the analytical curve $\epsilon = 0.221$, $T_a = 1300K$, and $V_{app} = 4 V$.	100
Fig 5.11 (b) Variation of cathode potential drop as a function of cathode temperature for different applied voltages marked on the curves. The dashed lines show the analytical behaviour.	101
Fig 5.12 (a) Variation of current density as a function of cathode temperature for different applied voltages, $\epsilon = 0.543$ $T_a = 1260K$ and run time = 8 hours.	104
Fig 5.12 (b) Variation of anode potential drop as a function of cathode temperature for different applied voltages, $\epsilon = 0.543$, $T_a = 1260K$ and run time = 8 hours.	105
Fig 5.13 (a) Variation of current density as a function of cathode temperature for different applied voltages, $\epsilon = 0.823$, $T_a = 1220K$, and run time = 4 hours	106
Fig 5.13 (b) Variation of cathode potential drop as function of cathode temperature for conditions similar to those of Fig 5.13(a)	107

	Page
Fig 5.13 (c) Variation of anode drop as function of cathode temperature for conditions similar to those of Figs 5.13 (a) and (b)	108
Fig 5.14 Variation of current density as a function of cathode temperature after 2 hours of channel run time. The dashed curve represents the analytically evaluated variation. $\epsilon = 0.823$, $T_a = 1060$ K and $V_{app} = 40V$.	110
Fig 5.15 (a) Variation of current density as a function of anode temperature for different applied voltages, $\epsilon = 0.747$, $T_c = 1180$ K and run time = 6 hours	114
Fig 5.15 (b) Variation of anode potential drop as a function of anode temperature for different applied voltages.	115
Fig 5.16 (a) Variation of current density as a function of anode temperature. The copper cathode has a matrix surface with 65 points and the copper anode has a planar surface, $\epsilon = 0.706$; $T_c = 1240$ K and run time = 2 hours.	116
Fig 5.16 (b) Variation of anode potential drop as a function of anode temperature. The electrode geometry and the experimental conditions are similar to those ^{of} Fig 5.16(a).	117
Fig 5.17 Variation of current density as a function of cathode temperature for a pair of planar stainless steel electrodes, $\epsilon = 0.503$ $T_a = 1570K$ and run time = 2.15 hours.	119
Fig 5.18 Variation of current density as a function of anode temperature for a pair of planar stainless steel electrodes, $\epsilon = 0.503$, $T_c = 1500K$ and run time = 7.0 hours.	120

	Page	
Fig 5.19	Variation of anode potential drop as a function of cathode temperature. The electrode geometry and experimental conditions are similar to those of Fig 5.17 .	122
Fig 5.20	Variation of anode potential drop as a function of anode temperature for a pair of planar Stainless steel electrodes. The experimental conditions are similar to those of Fig 5.18	123
Fig 6.1	Scanning electron micrograph of unused planer copper electrode surface before test run.	130
Fig 6.2	The Auger Emission Spectra of unused planar copper electrodes surface before the test run. Cu = 87.77%, O = 4.82%, C = 7.41%.	131
Fig 6.3	Scanning Electron Micrograph of the composite electrode surface after 16 hours of channel run, $\epsilon = 0.495$ and $T_c = T_a = 1000K$	133
	(a) Composite cathode surface.	
	(b) Composite anode surface.	
Fig 6.4	The Auger Emission Spectra of composite copper cathode surface after 16 hours of channel run, $\epsilon = 0.495$, $T_c = 1000K$. The spectra obtained at different locations on the surface are shown in Figs (a), (b) and (c).	134 135 136
Fig 6.5	The Auger Emission Spectra of composite copper anode surface after 16 hours of channel run, $\epsilon = 0.495$ and $T_a = 1000K$.	138
Fig 6.6	Scanning Electron Micrograph of a planar stainless steel electrode surface before the test run.	140

	Page
Fig 6.7 Scanning Electron Micrograph of composite stainless steel electrode surface after 8 hours of channel ^{run} $T_C = T_a = 1570K$, $\epsilon = 0.503$.	141
<p>(a) Composite stainless steel cathode.</p> <p>(b) Composite stainless steel anode.</p>	
Fig 6.8 The Auger Emission spectra of stainless steel electrode surface before the test run Fe = 67.87%; Cr = 18.09%, Ni = 6.59% and C = 7.42%.	142
Fig 6.9 The Auger Emission spectra of composite surface on stainless steel cathode after 12 hours of channel run time, $\epsilon = 0.503$ and $T_C = 1550K$.	144 145 146
Fig 6.10 Thermal behaviour of composite material under DTA run.	148

LIST OF TABLES

No.	Title	Page
3.1	Constituents of liquefied Petroleum-gas	35
3.2	Composition of Solid Potassium Carbonate used for seeding	40
3.3	Thermophysical Properties of Potassium Carbonate and its aqueous solution	46
5.1	Current Density and Electrode Potential Drop under different operating conditions	111
6.1	Concentration of Constituents as a Function of Depth on Composite Stainless Steel Cathode Surface	147

NOMENCLATURE

English letter symbols

A	Richardson's constant
A ₁	Area of cross-section of atomising tube
A ₂	Area of cross-section of atomising tube at nozzle
A _p	Effective area of probe for current conduction
b ₁ to b ₄	Constants
B	Magnetic field
C ₀	Concentration of aqueous seed solution (initially)
C _i	Concentration of i th species
C _s	Concentration of the Saturated Solution
C _{p0}	Specific heat of aqueous seed solution at constant pressure
C _{p1}	Specific heat of solid K ₂ CO ₃ at constant pressure
C _{p2}	Specific heat of liquid K ₂ CO ₃ at constant pressure
d	$\frac{e}{A}$ Separation between the probes
d _{vs}	volume to surface ratio of total droplets in a spray, i.e. sauter mean diameter

e	Electronic Charge
E	Electric field
f	Fractional radius ($= r/r_0$)
f_1	The ratio of the saturated seed droplet radii to mean radii ($=r_s/r_0$)
f_2	The ratio of the melted K_2CO_3 droplet radii to mean radii (r_M/r_0)
f_3	The ratio of the evaporated droplet radii to mean radii (r_E/r_0)
$F(v)$	A function of velocity
H_i	Peak to peak $\frac{e}{\lambda}$ hight of Auger emission
J	Total current density
J_e	Electronic current density
J_i	Ionic current density
k	Thermal conductivity of combustion products
k_B	Boltzmann's Constant
k_{el}	Thermal conductivity of electrode material
k_i	Thermal Conductivity of ith species
K_L	Loading parameter
l	Characteristic length

L_1	Latent heat of fusion of solid K_2CO_3
L_2	Latent heat of vaporisation of liquid K_2CO_3
L_s	Latent heat of saturated solution
m_0	Mass of the 15% aqueous K_2CO_3 solution
\dot{m}	Mass flow rate per min
m	Amount of water present in the seed solution
m_e/m_i	The ratio of electron to potassium ion mass
n	Total number of species in a mixture
n_e	Electron density
n_i	Ion density
n_{is}	Ion current density assuming local saha equilibrium
n_{is}	Random ion current density at cathode sheath edge.
$n_{es\infty}$	Electron density assuming local saha equilibrium
N	Number of the seed droplets
$N(E)$	Auger electron as a function of kinetic energy
P	Pressure
P_0	power output per unit volume
$P_{,s}$	Partial pressures of various species

q	Density of the convective flux falling on the drop and its average
Q_L	Volumetric flow rate of seed solution
Q_A	Volumetric flow rate of atomising oxygen
r	Radius of the seed droplet
r_0	Mean radii
r_s	Radii of the saturated solution
r_M	Radii of the melted drop (at 1164K)
r_E	Radii of the evaporating drop
R	load
s	Saturated solution
S_i	Sensitivity of the i th species for Auger emission
S_1 t_0	Equilibrium constants
S_5	
S_6	Constant
t	Time
Δt_i	total time taken by a droplet for evaporation ($\cong \Delta t$)
t_1 t_0 t_7	Time take by seed droplet during successive seven stages

T	Temperature
T ₀	Ambient temperature (303K)
T _S	Boiling point of saturated solution
T _M	Melting point of solid K ₂ CO ₃
T _E	Evaporation Temperature of liquid K ₂ CO ₃
T _∞	Main plasma temperature
T _a	Anode temperature
T _c	Cathode temperature
U	Velocity of the seeded combustion products
V _i	Ion thermal velocity
V	Relative velocity of the atomising oxygen gas w.r.t. aqueous seed flow rate
V ₁	Velocity of oxygen in atomising tube
V ₂	Velocity ^{of} oxygen at the nozzle of atomising tube
V _a	Anode potential drop
V _c	Cathode potential drop
V _{app}	Applied voltage
W _i	Mole fraction of ith species
X _L	Axial distance from the Burner

Greek Letter Symbols

ρ_0	Density of 15% K_2CO_3 Solution
ρ_1	Density of solid K_2CO_3
ρ_2	Density of liquid K_2CO_3 at 1795 K
ρ_s	Density of saturated seed solution
ρ_E	Density of liquid K_2CO_3 at 1945 K
ν_t	Total collision frequency
ν_{en}	Collision frequency of electron and neutral <i>particles</i>
σ	Electrical conductivity of seeded combustion plasma
σ_T	Surface tension of the seed solution
ϕ	Work function
ϵ	Weight per cent of Potassium
δ	Solid shell thickness of K_2CO_3
δ_c	Cathode electrostatic sheath thickness
δ_T	Thermal sheath thickness
α, β, γ	Constants

CONTENTS

	Page
ACKNOWLEDGEMENT	(iii)
PREFACE	(iv)
LIST OF FIGURES	(vi)
LIST OF TABLES	(xii)
NOMENCLATURE	(xiv)

CHAPTER 1

INTRODUCTION

1.1 MHD Power Generation	1
1.2 Role of Seed	4
1.3 Electrical conductivity	6
1.4 Current Conduction Phenomenon	7
1.5 Adsorption on Electrode Surfaces	11
1.6 Synopsis of the Present Work	12

CHAPTER 2

THEORETICAL ANALYSES

2.1 Introduction	17
2.2 Atomisation of Seed Solution	18

	Page
2.3 Evaporation of Atomised Seed Solution	18
2.4 Transport Properties of Seeded Combustion Products	26
2.5 Electrode Boundary Layers	29

CHAPTER 3

EXPERIMENTAL FACILITY AND DIAGNOSTICS

3.1 Introduction	34
3.2 Experimental System	34
3.2.1 Gas Control Unit	34
3.2.2 Burner	38
3.2.3 Seed Injection System	38
3.2.4 Test Section	47
3.2.5 Electrodes	49
3.3 Diagnostics	52
3.3.1 Temperature of Seeded Combustion Products	53
3.3.2 Electrical Conductivity	54
3.3.3 Seed Droplet Measurement	57

CHAPTER 4

SEED DROPLET EVAPORATION AND ELECTRICAL CONDUCTIVITY

4.1 Introduction	60
4.2 Distribution of Pneumatically Atomised Seed Droplet	61

	Page
4.3 Seed Evaporation Time	63
4.4 Temperature and Electrical Conductivity	70
4.5 Conclusions	82

CHAPTER 5

CURRENT CONDUCTION IN SEEDED COMBUSTION PLASMAS

5.1 Introduction	83
5.2 Planar Copper Electrodes	84
5.2.1 Temporal Behaviour of Potential Drop	92
5.2.2 Potential Distribution Between the Electrodes	94
5.2.3 Effect of Cathode Temperature	97
5.2.4 Effect of Anode Temperature	112
5.3 Matrix Copper Cathode	113
5.4 Stainless Steel Electrodes	118
5.5 Conclusions	124

CHAPTER 6

CHARACTERISATION OF ELECTRODE SURFACES

6.1 Introduction	126
6.2 Experimental Techniques	126

	Page
6.2.1 Auger Electron Spectroscopy (AES)	126
6.2.2 Scanning Electron Microscopy (SEM)	128
6.2.3 Differential Thermal Analysis (DTA)	128
6.3 Results and Discussion	129
6.3.1 Copper Electrodes	129
6.3.2 Stainless Steel Electrodes	139
6.3.3 Thermal Behaviour of Composite layer	143
6.4 Conclusions	149

APPENDECES

Appendix A Computer Programme for the Evaluation of Seed Droplet Evaporation Time.	150
Appendix B Flow Chart for Composition, Temperature and Electrical Conductivity Calculations.	151
Appendix C Computer Programme for the case of Thermionically Emitting Cathode.	153

REFERENCES

156

BIO-DATA

166

REPRINTS/PREPRINTS